Available online at www.sciencedirect.com
SCIENCE DIRECT
Solid State Ionics 177 (2006) 931–938
SOLID STATE IONICS
www.elsevier.com/locate/ssi

Performance and durability of Ni-coated YSZ anodes for intermediate temperature solid oxide fuel cells

Sun-Dong Kim [a], Hwan Moon [a], Sang-Hoon Hyun [a,*], Jooho Moon [a], Joosun Kim [b], Hae-Weon Lee [b]

[a] School of Advanced Materials Science and Engineering, Yonsei University, Seoul 120-749, South Korea
[b] NMRC, Korea Institute of Science and Technology, Seoul 136-791, South Korea

Received 29 November 2005; received in revised form 10 February 2006; accepted 14 February 2006

Abstract

NiO-coated YSZ composite powders were synthesized through the Pechini process in order to improve the performance and durability of SOFC anodes. Their microstructures and electrical properties have been investigated with thermal and redox cycling tests. The coverage of NiO crystals on the YSZ surface could be modulated by controlling the composition of the reaction mixture and the ratio of NiO and YSZ. Ni–YSZ electrodes were manufactured by sintering the die-pressed NiO–YSZ pellet at 1400 °C for 3 h, followed by reducing it to 800 °C under hydrogen atmosphere. The anode made from NiO/YSZ composite powder, which has a high homogeneity and plenty of contact sites between Ni and YSZ, has an excellent tolerance against thermal and redox cycling. The maximum power density of a single cell made from NiO/YSZ composite powder was 0.56 W cm^{-2} at 800 °C in reactive gases of humidified hydrogen and air. It can be concluded that the functional NiO/YSZ composite powder will suppress the degradation of anodes and enhance the long-term and redox stability of the unit cell at elevated temperatures.

Keywords: Solid oxide fuel cell; Ni/YSZ anode; Composite powder; Redox cycling; Thermal cycling

1. Introduction

The recent commercial requirement for SOFC is that it maintain a life time of over 40,000–50,000 h. Consequently, it is obvious that only small degradation rates are acceptable [1]. It is widely believed that the instability of the electrode microstructure leads to the decrease in SOFC performances. This is particularly true for the Ni–YSZ cermet. Owing to advantages such as high electrical conductivity, catalytic activity for fuel oxidation, and mechanical/chemical compatibility with other components, it is the most adequate option for operation with clean H_2 or fully reformed fuel [2,3]. At elevated temperature, it is natural that metal phases in the cermet have a tendency to decrease the surface area and aggregate. Though the YSZ in the cermet prevents the coarsening of phases, the agglomeration and the coarsening of fine nickel grains grow significantly due to the poor adhesion of metal to ceramic material (Ni/YSZ contact angle: 117° at 1500 °C) [4]. Another big problem that causes trouble to the reliability of SOFC system is the redox stability of the Ni–YSZ anode. The cyclic reduction and oxidation (redox) by the system shutdown and/or the fuel supply interruption will lead to a large volume change of Ni to NiO, which affects the microstructure of the Ni/YSZ interface and results in the performance degradation or the catastrophic failure of the cermet anode [4–11].

The performance of the Ni–YSZ cermet is critically dependent on the microstructure and the distribution of Ni and YSZ phases in the cermet. This in turn is closely related to the characteristics of the NiO and YSZ powders and the fabrication process. Mogensen et al. [12] has shown that the performance of the cermet anode is closely related to the grain size combination of Ni and YSZ. They reported that the cermet structure, consisting of a YSZ network of small particles, shared large three phase boundaries (TPBs) with Ni particles and with small diffusion lengths for reacting species, combined with larger YSZ grains as media of oxide ions transfer. Their studies mainly examined the size effects of constituent particles on the

* Corresponding author. Tel.: +82 2 2123 2850; fax: +82 2 365 5882.
E-mail address: prohsh@yonsei.ac.kr (S.-H. Hyun).

0167-2738/$ - see front matter © 2006 Elsevier B.V. All rights reserved.
doi:10.1016/j.ssi.2006.02.007

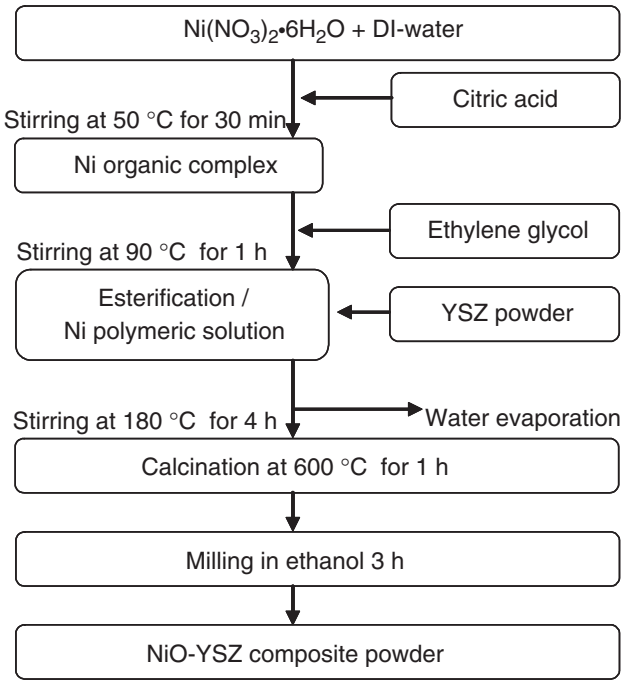

Fig. 1. Experimental flow chart for the synthesis of NiO/YSZ composite powder.

performance of cermet anodes, focusing little on the powder process. On the other hand, Fukui et al. [13] have studied the application of the YSZ-coated nickel powder for the long-term durability as well as higher electrochemical activity of the Ni–YSZ cermet anodes [14–18]. Their results indicated that composite powders have high homogeneity and large TPBs which cause low anode polarization and high electrochemical activity. The problem, then, is the relationship between the durability of Ni–YSZ electrode via controlling the coarsening of Ni particle and the dimensional change in long term operations (i.e. thermal/redox cycling) at elevated temperatures. In contrast with the works of Fukui [13], fine nickel grains, due to their high catalytic activity, help percolation and electrochemical activity. Moreover, composite powder, composed of both the fine and coarse YSZ particles as core material, is beneficial to the mechanical strength of and thermal expansion coefficient (TEC) match for the cermet anode.

Thus, the aim of this paper is to achieve high homogeneity, high performance, long-term durability, and thermal/redox cycling stability of the cermet anodes made from NiO/YSZ composite powder composed of nano-sized NiO crystallized on YSZ powder. Additionally, the relationships between anode performance and starting material (i.e. commercial NiO–YSZ mixing powder and NiO/YSZ composite powder) were analyzed, as were their effects on the improvement of SOFC performance.

2. Experimental

2.1. Preparation of the NiO/YSZ composite powder and the single cell

The NiO/YSZ composite powder was prepared through the Pechini process, and the synthetic procedure adopted for the preparation of NiO/YSZ composite powder (40 vol.% Ni–YSZ) is schematically shown in Fig. 1. The microstructure (i.e. porosity, pore size, etc.) and mechanical property of NiO–YSZ anode substrates were modulated by using the binary particle size of YSZ powders (Tosoh Co. 0.3 μm and Millennium Chemicals Inc., 10 μm), hereinafter labeled fine and coarse powder respectively. $Ni(NO_3)_2 \cdot 6H_2O$ (Junsei Chemical Co.) and citric acid (Junsei Chemical Co.) was dissolved in DI-water at 60 °C for the formation of nickel-citric acid organic complex. YSZ and ethylene glycol (Duksan Chemical Co.) was then added to the Ni nitrate aqueous solution at the mole ratio of 1:4 between citric acid and ethylene glycol. The polymeric solution precipitated as viscous resin on the YSZ particles via esterification and condensation. Vigorous stirring was necessary to prevent the settling or the agglomeration of the YSZ particles. Furthermore, the resin was dried at 180 °C for 4 h and ash colored intermediates was obtained. The resulting polymeric intermediates were calcined at 600 °C and milled in ethanol to obtain nano-sized NiO coated YSZ powder.

The anode powders were then compacted under uni-axial pressure to form a disc. The dimensions of green anode discs were 38 mm in diameter and 1.2 mm in thickness. The green anodes were pre-sintered at 1300 °C for 3 h. The YSZ(TZ-8YS, Tosoh, Japan) slurry was then applied onto the anode via dip-coating and

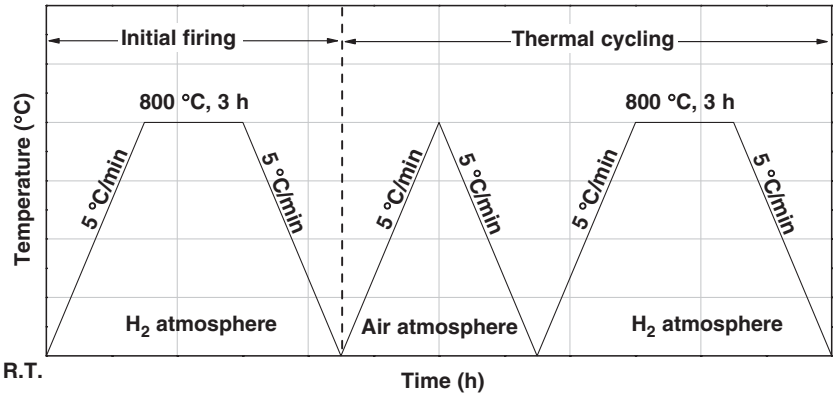

Fig. 2. Temperature profile for initial heat treatment and subsequent thermal cycling in the reduction/oxidation atmosphere.

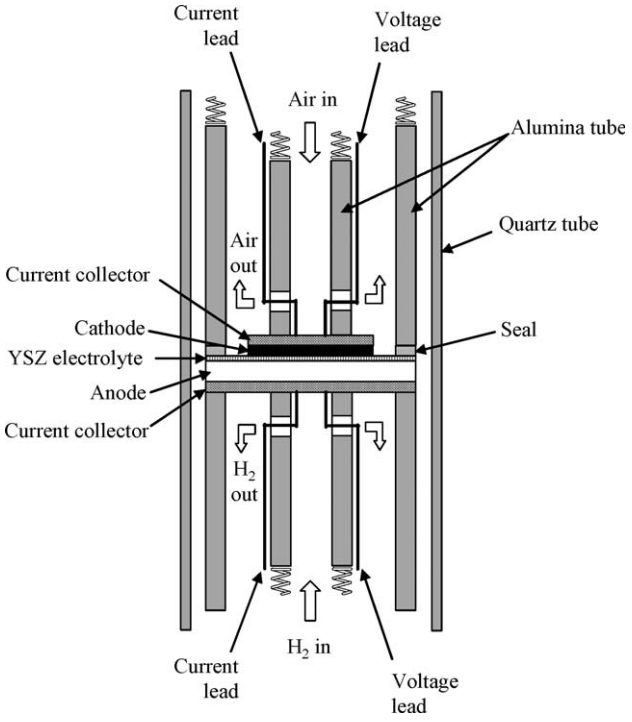

Fig. 3. Configuration of a test cell.

sintered at 1400 °C for 3 h to achieve a thin (<7 μm) and dense YSZ electrolyte film. The method employed for the synthesis of a thin and dense YSZ electrolyte film via dip-coating process has been reported in our previous work [19]. The cathode paste was prepared using $La_{0.8}Sr_{0.2}MnO_3$ (LSM: Praxair, USA) and YSZ (TZ-8YS, Tosoh, Japan) in a weight ratio of 50:50. The cathode layer was screen-printed on the anode-supported electrolyte with an active area of 1.5 cm^2 and thickness of 30 μm. The cathode layer was sintered at 1150 °C for 3 h.

2.2. Thermal/redox cycling tests

The microstructure stabilities of Ni based electrode were evaluated via thermal cycling tests under redox atmosphere as depicted in Fig. 2. Ni–YSZ anodes were manufactured by sintering the die-pressed NiO–YSZ pellet at 1400 °C for 3 h, followed by reduction at 850 °C under a hydrogen atmosphere (20 cm^3 min^{-1}). After that, thermal cycling was conducted under air atmosphere for oxidation at 800 °C and under hydrogen atmosphere for re-reduction at 800 °C for 3 h successively. Heating was at a rate of 5 °C min^{-1}. Each time after thermal cycling, the microstructures of Ni–YSZ cermet were examined by an optical microscope. The nickel grain size was evaluated by image analysis using Image-Pro (Media Cybernetics, USA). The degradation of anodic performance was investigated by measuring the electrical conductivity of electrodes during thermal cycling.

2.3. Characterizations

The crystalline phases of anode materials were analyzed by X-ray diffractometry (Rint 2700, Rigaku Co., Japan). The microstructure of NiO/YSZ composite powders was observed with a scanning electronic microscopy (SEM; Model S4200, Hitachi, Ltd., Japan). Interfacial bonding state of NiO/YSZ composite powder was characterized with a X-ray photoelectron spectroscopy (XPS) using the VG Scientific ESCALAB 220i-XL system (Non-monochromated Al Ka source, $h\nu$=1486.6 eV). The surface charge variations of composite powder that depended on the solution pH were measured using a zeta-potential analyzer (BI-Particle sizer ZPA, USA). The electrical conductivity of Ni–YSZ cermet was measured by DC 4-prove techniques with a current source unit (Keithley 224, USA) and a multi-meter (Iwatsu SC-7401, Japan).

The configuration of the test cell is shown in Fig. 3. Pt gauze supplied from Alfa (52 mesh, 0.1 mm wire) was used as a current collector. The current collectors were spring loaded, as depicted in Fig. 3. The performances of anode supported single cell were evaluated at various temperatures (700–800 °C) in reactive gases of humidified hydrogen (200 cm^3 min^{-1}) with 3% H_2O on the anode side and air (300 cm^3 min^{-1}) on the cathode side. *I–V* characterization and ac impedance measurements were conducted with a Solatron 1260 frequency analyzer and a Solatron 1287 interface. The ac impedance spectra in the frequency range of 0.1–10^5 Hz, with an excitation voltage of 10 mV, were taken to ensure a linear response.

3. Results and discussion

3.1. Characteristics of NiO/YSZ composite powder

The crystalline phase variations of NiO/YSZ composite powders that depend on the synthetic procedure are shown in Fig. 4. The polymeric intermediates that contained nickel precursor were confirmed to be amorphous phase. After

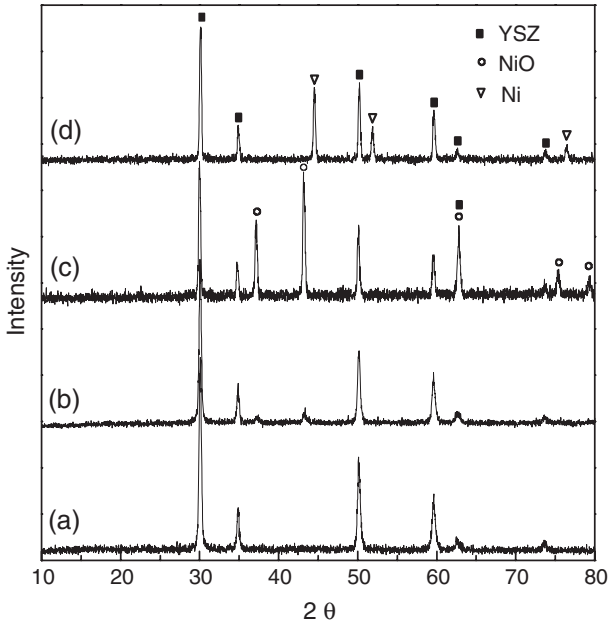

Fig. 4. XRD patterns of (a) resin embedded NiO/YSZ composite powder, (b) NiO/YSZ composite powder calcined at 600 °C for 1 h, (c) NiO–YSZ electrode sintered at 1400 °C for 3 h, and (d) Ni–YSZ electrode reduced at 800 °C in H_2.

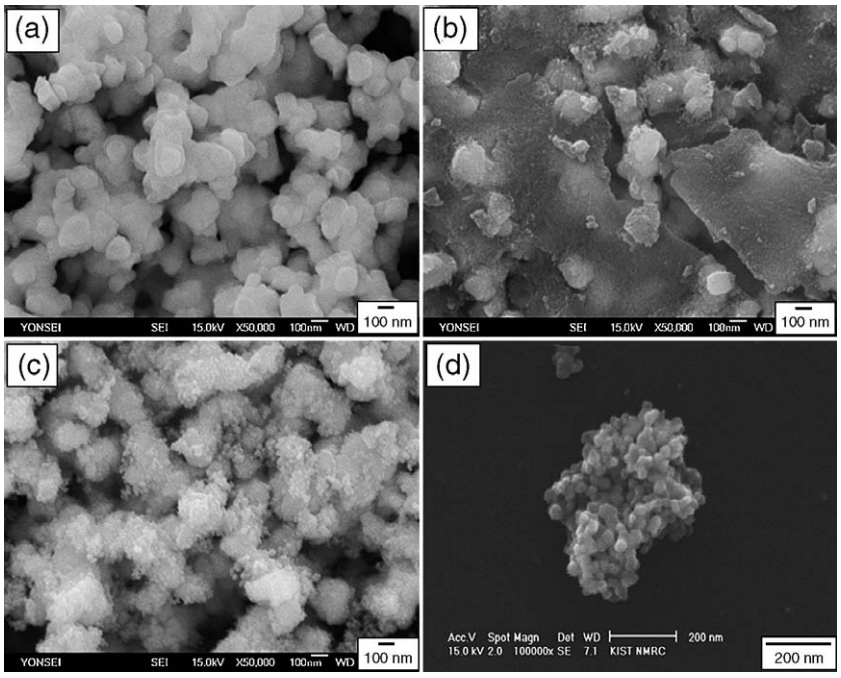

Fig. 5. SEM micrographs of NiO–YSZ composite powder: (a) commercial YSZ powder (TZ-8YS, Tosoh Co.), (b) resin embedded NiO/YSZ composite powder, (c) NiO/YSZ composite powder calcined at 600 °C for 1 h, and (d) NiO/YSZ composite particle.

calcination, the NiO was crystallized and the crystallinity improved after sintering at 1400 °C. The sharp diffraction patterns were perfectly matched with crystal structures for NiO and YSZ (Fig. 4c). The NiO diffraction peaks disappeared after reduction at 800 °C in H_2 and only peaks for Ni and YSZ were present, which means the NiO–YSZ electrode was perfectly reduced to a Ni–YSZ electrode.

Fig. 5 shows SEM micrographs of NiO/YSZ composite powders. The configuration of the powder is primarily nano-sized (20–~30 nm) NiO coated on YSZ (<300 nm) particles. Before calcination, the nickel containing organic complex existed as an amorphous resin as can be seen in Fig. 5b. The thermal decomposition terminated completely at 600 °C, and the resulting NiO cohered with the YSZ (Fig. 5c and d). The coverage of NiO particles on YSZ could be controlled by regulating the molar ratio of $Ni(NO_3)_2 \cdot 6H_2O$ to YSZ. Taking the sinterbility of NiO and YSZ particles into consideration, it is preferable that the NiO composite layers are built up as porous multi-layers.

In this composite process, one concern would be whether the coherence between NiO and the YSZ particles arises from physical or chemical adsorption. Obviously, the deposited NiO particles were not detached from the YSZ particles even after ball-milling overnight in ethanol (Fig. 5d). Fig. 6 shows the XPS spectra of Zr 3d core level for pure YSZ, NiO–YSZ mixing powder, and NiO–YSZ composite powder, and the corresponding binding energy and the full width at half maximum (FWHM) values are summarized in Table 1. The Zr 3d doublet spectrum can be resolved into two peaks, i.e. Zr $3d_{5/2}$ and Zr $3d_{3/2}$ at a binding energy of 181.8 eV and 184.2 eV, respectively, similar to those reported by Pomfret et al. [20]. The FWHM in Fig. 6c exhibits a larger value than those in Fig. 6a and b. This indicates the existence of a different kind of stable bonding and corresponding interaction force [21–23]. The bonding state of the YSZ–NiO interface is proposed to be the atomic structure of –Zr–O–Ni–. These chemical bonds have little influence on the overall crystalline phases (see Fig. 4) because the bonding sites are limited at the interface between

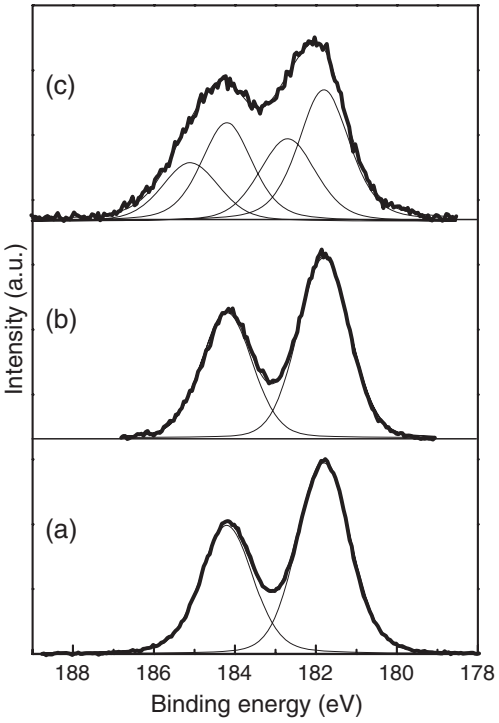

Fig. 6. Zr 3d core-level XPS spectra: (a) YSZ, (b) NiO–YSZ mixing powder, and (c) NiO/YSZ composite powder.

Table 1
XPS binding energies (EB) and FWHM values of YSZ, NiO–YSZ mixing powder, and NiO/YSZ composite powder

System	Zr $3d_{5/2}$		Zr $3d_{3/2}$		O 1s	
	E_B (eV)	FWHM (eV)	E_B (eV)	FWHM (eV)	E_B (eV)	FWHM (eV)
Yttria-stabilized zirconia	181.8	1.5	184.2	1.5	529.8	17
NiO–YSZ mixing powder	181.8	1.5	184.2	1.5	529.8	17
NiO–YSZ composite powder	181.8	2.0	184.2	2.0	529.8	2.3

YSZ and NiO. However, the composite powder has high homogeneity and plenty of contact sites between Ni and YSZ. Therefore, higher energy is needed to break the attraction between Ni and YSZ and to have a mobility of Ni phase in the cermet at high temperature.

Fig. 7 shows the effect of solution pH on the zeta-potential of powders prepared in 1 mM KNO_3 solution. The iso-electric points (IEP) of NiO and YSZ were 3.0 and 4.8, respectively. The IEP of NiO–YSZ mixing powder is about 3.9 which is located between the IEP of NiO and YSZ. The surface electro-kinetic behavior entirely depends on the property of surfaces. In the case of NiO–YSZ composite powder, the NiO composite layer hides the surface of YSZ, and has an electro-kinetic behavior very similar to that of NiO. This indicates that the composite powder has a configuration of NiO coated on YSZ core.

3.2. Characteristics of Ni–YSZ electrodes made from NiO–YSZ composite powder

The porosity of Ni-based electrodes change during reduction because there is a difference in the specific volume between nickel and nickel oxide. The porosity variations of Ni–YSZ electrode is demonstrated in Fig. 8. The anode must have sufficient porosity to allow gas transport to the reaction site. Enough mass transport can be performed when the porous anode consist of mostly open pores and the porosity is over 35–40%. In the conventional process, the porous

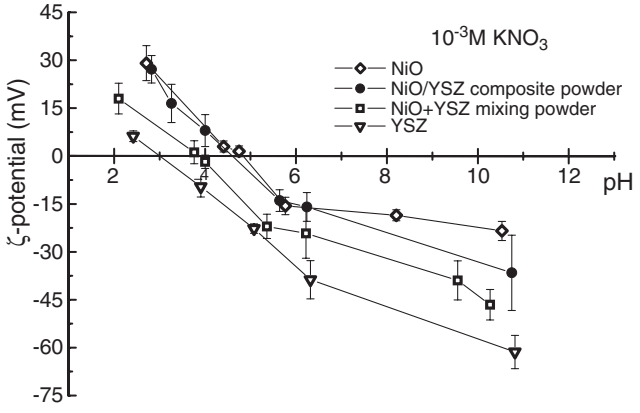

Fig. 7. Porosity variations of anode substrate with different particle size ratio.

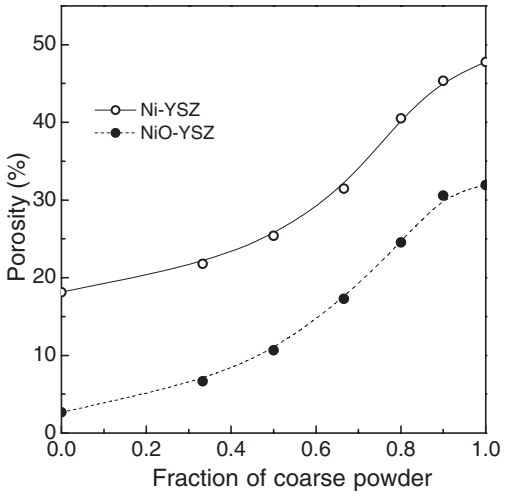

Fig. 8. Mechanical strength of anode substrate with different particle size ratio determined under 3-point bending test.

anodes were fabricated by using pore-formers (i.e. carbon, polymer, etc.) as templates. However, these pore-formers lack in uniformity due to the fundamental problem of mixing well and leave ashes even after pyrolysis/sintering. Therefore, our approach is to tailor the porosity of the anode substrate not by using the pore-former but by using the size effects of powders. The porosity of anodes increased with the content of the coarse powder, for example, when the fraction of the coarse powder was 0.8 (fine 20%/coarse 80%) the porosity of Ni–YSZ anode was 40%. These combinations of powders also influence the mechanical property of the anode, as can be seen in Fig. 9. The mechanical strength was found to decrease with the increasing fraction of the coarse powder, because the sinterbility of the coarse powder is inferior to the fine powder. Therefore, considering the basic requirement of the porosity and mechanical strength, the constitution of composite NiO–YSZ powder was optimized at a fraction of 20% fine powder and 80% coarse powder, and the porosity and mechanical strength of Ni–YSZ anode was 40% and 27 MPa, respectively.

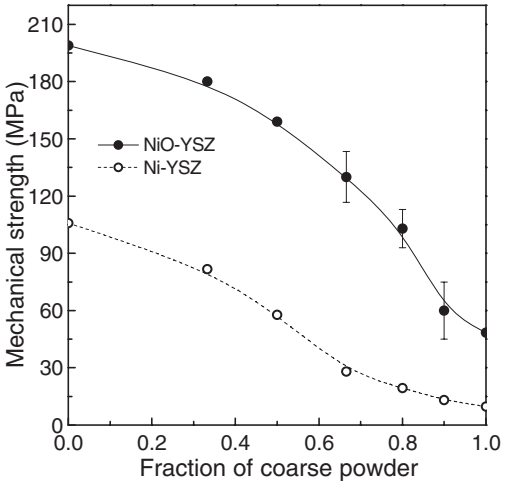

Fig. 9. NiO/YSZ composite effects on the variations of zeta-potential.

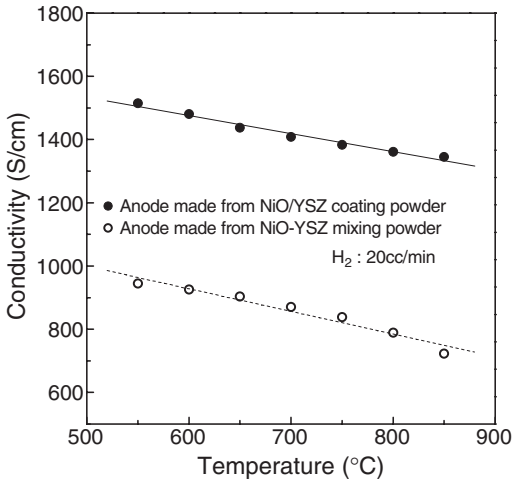

Fig. 10. Electrical conductivity of anode substrate as a function of temperature.

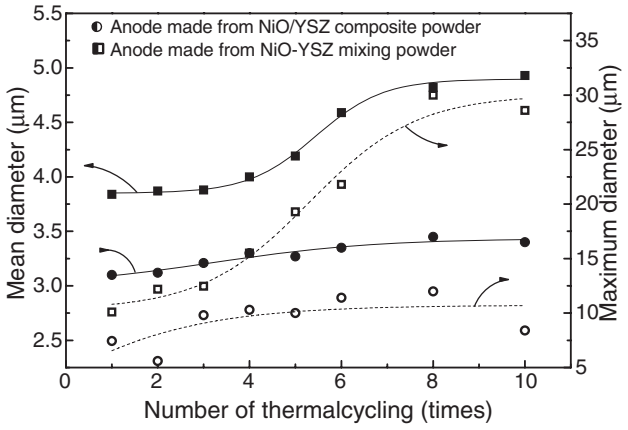

Fig. 12. Quantitative analysis of Ni coarsening effects depending on thermal cycling.

The temperature dependence for the electrical conductivity of Ni–YSZ electrode is shown in Fig. 10. For Ni based electrodes, the electrical conductivity is entirely dependant on the connection through the nickel phase, and generally a higher Ni content is beneficial for the higher electrical conductivity. However, this leads to the instability of microstructure and low mechanical strength of anodes. Consequently, the content of Ni must be optimized; this is based on the performance and durability as an electrode. In our case, when the same Ni content (40 vol.% Ni–YSZ) was used, the electrical conductivity of anode made from NiO–YSZ composite powder was higher than the conventional anode. This is due to the effective percolation through the Ni phase and the uniform microstructure of Ni–YSZ anode made from NiO–YSZ composite powder.

3.3. Durability under thermal/redox cycling tests

After each thermal cycling, the microstructure and electrical conductivity variations were observed to characterize the amount of microstructure degradation. The Ni coarsening effects that depend on thermal cycling were analyzed by the quantitative image analysis technique, described in the works of Simwonis et al. [24,25].

The microstructure changes of Ni–YSZ anode along with the progress of thermal cycling are shown in Fig. 11. Phases can be separated from the optical image on the basis of their brightness, where the bright phases are Ni and the dark phases are YSZ and pores. The nickel coarsening in anodes made from NiO–YSZ mixing powder (Fig. 11a–c) is distinguishable even at the early stage of thermal cycling. The observed microstructure changes

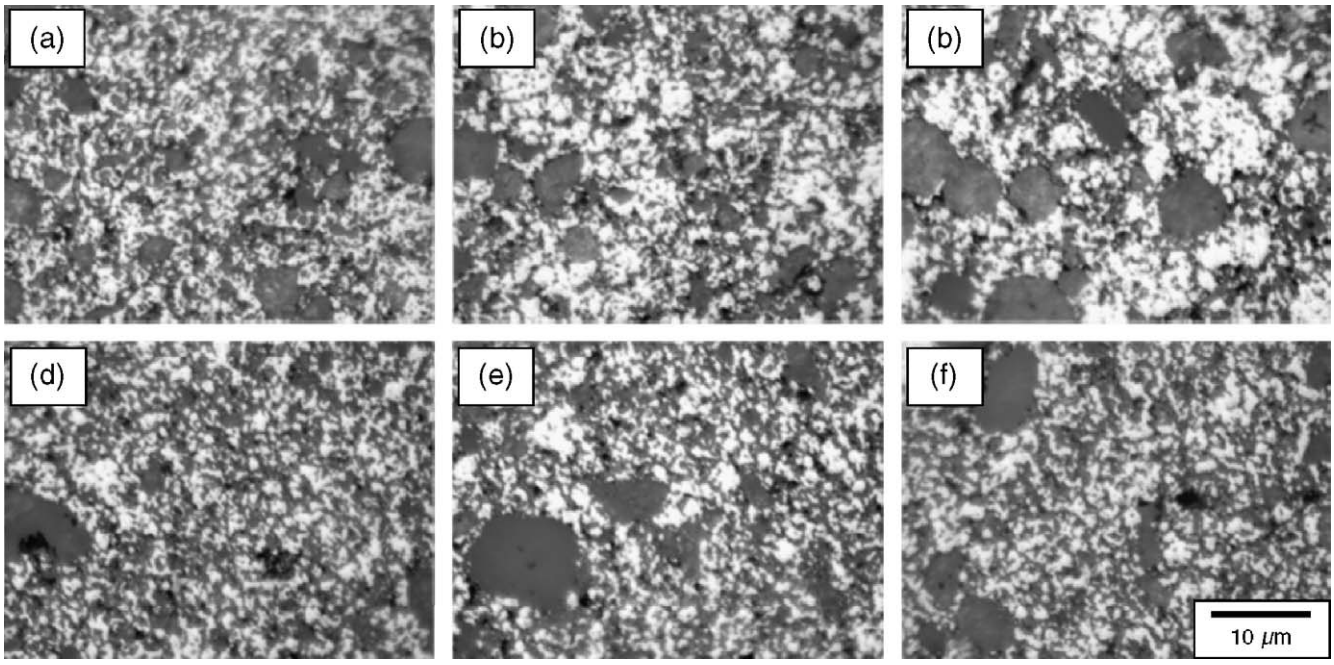

Fig. 11. Microstructure (optical image) variations of Ni–YSZ anodes depending on the number of thermal cycling: (a) anode made from NiO–YSZ mixing powder after thermal cycling one time, (b) after thermal cycling five times, (c) after thermal cycling ten times, (d) anode made from NiO/YSZ composite powder after thermal cycling one times, (e) after thermal cycling five times, and (f) after thermal cycling ten times.

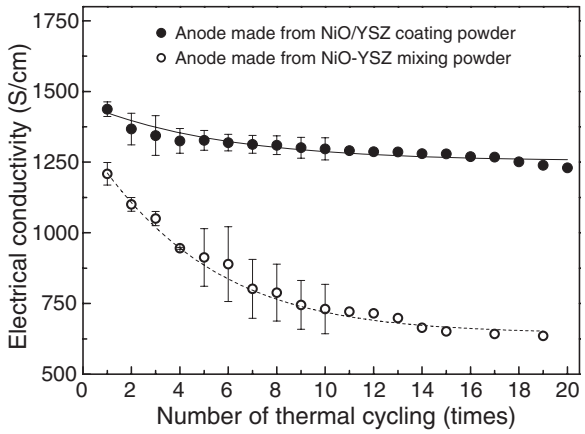

Fig. 13. Electrical conductivity variations of anodes depending on thermal cycling.

in the electrode are due to Ni sintering at an elevated temperature. However, there is little change in the microstructure of Ni–YSZ anode made from NiO–YSZ composite powder during the thermal cycling. The size variations of the Ni phase during the thermal cycling are summarized in Fig. 12. There was a rapid increase in the diameter of nickel phases in anode made from NiO–YSZ mixing powder. The maximum diameter, which is an index of cohesion, grew three times during the 10 thermal cyclings. On the other hand, the size and distribution of the nickel phase in anode made from NiO–YSZ composite powder remained constant against the thermal and redox cycling. This is due to the high activation energy which is required for the rearrangement of the Ni phases in the cermet for the interaction force by cohesion of NiO and YSZ particles.

Fig. 13 shows the electrical conductivity variations of Ni–YSZ electrode depending on the number of thermal cycling. The electrical conductivity represents the percolation of Ni phases. Uniform distribution of Ni phase is preferable for high electrical conductivity, and the electrical conductivity of the anode made from NiO–YSZ mixing powder decreases

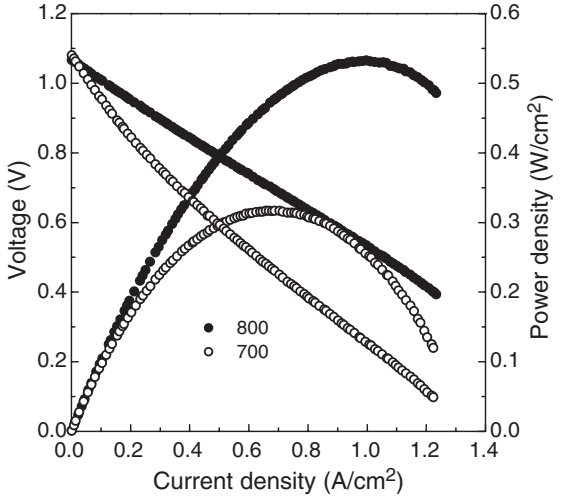

Fig. 14. The *I–V* characteristics of the anode supported cell made from NiO/YSZ composite powder in reactive gases of humidified hydrogen (200 cm^3 min^{-1}) with 3% H_2O and air (300 cm^3 min^{-1}).

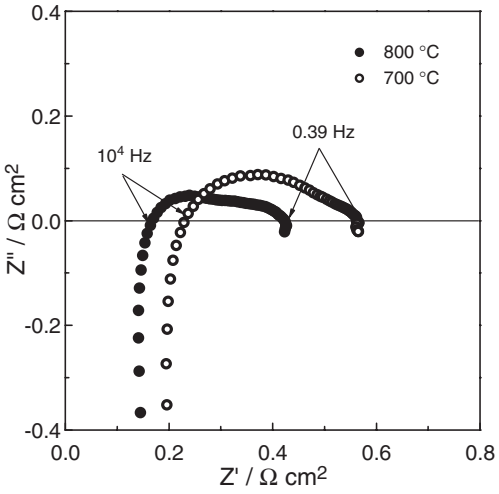

Fig. 15. The impedance spectra of the anode supported cell made from NiO/YSZ composite powder in reactive gases of humidified hydrogen (200 cm^3 min^{-1}) with 3% H_2O and air (300 cm^3 min^{-1}).

continuously with the progress of thermal cycling. After 20 thermal cyclings, the electrical conductivity decreased from 1208.8 S cm^{-1} to 635.4 S cm^{-1} (47% decreases). However, the electrical conductivity of the anode made from NiO–YSZ composite powder shows little change during the 20 thermal cycling tests (10% decrease). These results exactly correspond with the tendency of microstructure variations of Ni–YSZ anodes depending on thermal cycling (see Figs. 11 and 12).

3.4. Single cell performance

I–V characteristics of a single cell which is made from NiO–YSZ composite powder are shown in Fig. 14. The maximum power density of the cell was 0.56 W cm^{-2} at 800 °C and 0.32 W cm^{-2} at 700 °C in humidified hydrogen (200 cm^3 min^{-1}) as the fuel and air as the oxidant (300 cm^3 min^{-1}). The parameters of the anode side that affect the single cell performance are its microstructure, pore/pore-size distribution, three phase boundary, anode/electrolyte interface, and anode thickness, etc. These loss parameters, which result in the voltage loss of a cell at a given operating current density, include concentration/activation polarization of electrode and ohmic polarization of anode/electrolyte interfaces. From the results of ac impedance spectroscopy in Fig. 15, at least two processes contribute to the polarization resistance (0.17 Ω cm^2 at OCV at 800 °C). In our cell, the microstructure of the anode is designed for effective pore structure and expanded TPBs. Therefore, the single cell performance improved through low polarization resistance and its high performance at a low temperature (0.32 W cm^{-2} at 700 °C) enabled the intermediate temperature operations of SOFCs.

4. Conclusions

The current study investigated the performance and the durability of the cermet anode made from NiO–YSZ composite powder composed of nano-sized NiO crystallized onto the

surface of YSZ. The composite powder was successfully fabricated applying the Pechini process. The anode substrate, as an electrode, satisfied fundamental requirements such as mechanical strength (>27 MPa), porosity (≈40%), and electrical conductivity (>1400 S cm^{-1} at 800 °C) due to the effective percolation among the three phases (Ni, YSZ, and pores) and the uniform microstructure. The maximum power density of the single cell made from NiO–YSZ composite powder with an active area of 1.5 cm^2 was 0.56 W cm^{-2} at 800 °C in reactive gases of humidified hydrogen (200 cm^3 min^{-1}) and air (300 cm^3 min^{-1}). The anode made from NiO–YSZ composite powder, which has high homogeneity and plenty of contact sites between Ni and YSZ, has an excellent tolerance against thermal and redox cycling. The functional NiO–YSZ composite powders suppress the degradation of anodes and enhance the long-term and redox stability of the unit cell at elevated temperatures.

Acknowledgements

This work was supported by the Core Technology Development Program for Fuel Cell of Ministry of Science and Technology and Korea Institute of Science and Technology Evaluation and Planning.

References

[1] S. Primdahl, M. Mogensen, J. Appl. Electrochem. 30 (2000) 247.
[2] C.H. Lee, C.H. Lee, H.Y. Lee, S.M. Oh, Solid State Ionics 98 (1997) 39.
[3] M. Mogensen, S.P. Primdahl, M.J. Jorgensen, C. Bagger, J. Electroceram. 5 (2) (2000) 141.
[4] S.P. Jiang, J. Mater. Sci. 38 (2003) 3775.
[5] D. Waldbillig, A. Wood, D.G. Ivey, J. Power Sources 145 (2005) 206.
[6] Y.L. Liu, C. Jiao, Solid State Ionics 176 (2005) 435.
[7] Y.C. Hsiao, J.R. Selman, Solid State Ionics 98 (1997) 33.
[8] H. Koide, Y. Someya, T. Yoshida, T. Maruyama, Solid State Ionics 132 (2000) 253.
[9] R. Wilkenhoener, R. Vasen, H.P. Buchkremer, D. Stover, J. Mater. Sci. 34 (1999) 257.
[10] J.H. Lee, H. Moon, H.W. Lee, J. Kim, J.D. Kim, K.H. Yoon, Solid State Ionics 148 (2002) 15.
[11] B.Q. Xu, J.M. Wei, Y.T. Yu, Y. Li, J.L. Li, Q.M. Zhu, J. Phys. Chem., B 107 (2003) 5203.
[12] M. Mogensen, S. Skaarup, Solid State Ionics 86–88 (1996) 1151.
[13] T. Fukui, K. Murata, S. Ohara, H. Abe, M. Naito, K. Nogi, J. Power Sources 125 (2004) 17.
[14] J.W. Moon, H.L. Lee, J.D. Kim, G.D. Kim, D.A. Lee, H.W. Lee, Mater. Lett. 38 (1999) 214.
[15] P. Duran, J. Tartaj, F. Capel, C. Moure, J. Eur. Ceram. Soc. 23 (2003) 2125.
[16] S.K. Pratihar, A.D. Sharma, R.N. Basu, H.S. Maiti, J. Power Sources 129 (2004) 138.
[17] F.H. Wang, R.S. Guo, Q.T. Wei, Y. Zhou, H.L. Li, S.L. Li, Mater. Lett. 58 (2004) 3079.
[18] G. Gen, Z.X. Guo, C.K.L. Davies, Scr. Mater. 43 (2000) 307.
[19] S.D. Kim, S.H. Hyun, J. Moon, J.H. Kim, R.H. Song, J. Power Sources 139 (2005) 67.
[20] M.B. Pomfret, C. Stolts, B. Varughese, R.A. Walker, Anal. Chem. 77 (2005) 1791.
[21] M.K. Dongare, K. Malshe, C.S. Gopinath, I.K. Murwani, E. Kemnitz, J. Catal. 222 (2004) 80.
[22] E. Symianakis, S. Ladas, G.A. Evangelakis, Appl. Surf. Sci. 217 (2003) 239.
[23] H.L. Zhang, D.Z. Wang, B. Yang, N.K. Huang, Phys. Statatus Solidi, A 160 (1997) 145.
[24] D. Simwonis, F. Tietz, D. Stover, Solid State Ionics 132 (2000) 241.
[25] D. Simwonis, A. Naoumidis, F.J. Dias, J. Linke, A. Moropoulou, J. Mater. Res. 12 (6) (1997) 1508.